Eur. Phys. J. Special Topics **226**, 1169–1176

DOI: 10.1140/epjst/e2016-60207-7

THE EUROPEAN PHYSICAL JOURNAL SPECIAL TOPICS

Regular Article

Enhancement of heat transfer rate on phase change materials with thermocapillary flows

Santiago Madruga[1,a] and Carolina Mendoza[2]

[1] Department of Applied Mathematics to the Aerospace Engineering, School of Aerospace Engineering, Universidad Politécnica de Madrid (UPM), Plaza Cardenal Cisneros 3, 28040 Madrid, Spain
[2] Instituto de Ciencias Matemáticas, CSIC-UAM-UC3M-UCM, C/ Nicolás Cabrera 15, Campus Cantoblanco UAM, 28049, Madrid, Spain

Received 30 June 2016 / Received in final form 29 July 2016
Published online 2 May 2017

Abstract. We carry out simulations of the melting process on the phase change material n-octadecane in squared geometries in the presence of natural convection and including thermocapillary effects. We show how the introduction of thermocapillary effects enhances the heat transfer rate, being the effect especially relevant for small Bond numbers. Thus induction of Marangoni flows results in a useful mechanism to enhance the typical slow heat transfer rate of paraffin waxes in applications of energy storage or passive control management.

1 Introduction

The important environment problems of traditional sources of energy have promoted an intense and increasing interest in energy efficiency and development of renewable and clean sources of energy. It has realized that to achieve this goal producing energy must be accompanied with systems to store it, like thermal energy storage systems.

The usage of Phase Change Materials (PCM) is a low cost, environmentally friendly and safe solution for thermal energy storage. PCM use the large latent heat of the solid/liquid phase transition to store a large amount of energy during melting or release it during solidification, changing very little the temperature during the transition. Currently, there are hundredths of PCM known -as organic, inorganic and eutectics- with a wide range of melting points (from temperatures below zero to hundredths of Celsius degrees).

Among PCM the paraffin waxes are very well suited for thermal storage at room temperatures, and they are widely used for improving energy efficiency in buildings [1]. Interesting, they are used as well within space crafts in microgravity for the conservation of samples, food and electronic thermal energy management [2,3]. However, a major issue in thermal regulation with most PCM, including paraffins, is their low conductivity, usually $< 1\,\mathrm{W\,m^{-1}\,K^{-1}}$. This leads to very long times during the heat storage and discharge phases, reducing their applicability.

[a] e-mail: santiago.madruga@upm.es

On ground applications, the main choice to reduce the problem of low conductivity is to promote convective motions within the liquid phase of the PCM. Convective motions driven by gradients of density induced by differences of temperature enhance the heat transfer rate about an order of magnitude with respect to conductive heat transport. Another approach to accelerate the heat transfer is to place a large area of PCM in contact with high conductivity materials, like metallic fins or metallic foams [4]. Whereas this solution is applicable under microgravity conditions, it increases the mass and size of the devices, and the absence of convective driving may not be fully compensated.

Prompted by the above considerations a mechanism to enhance the heat transfer on PCMs without increasing mass and volume, is to maximize the Marangoni flow induced by thermal gradients of surface tension. We aim at studying the melting dynamics of the paraffin n-octadecane, which exhibits a solid/liquid phase change at 26.1 °C and is widely used due to its stability and suffers no undercooling.

In Section 2 we present the governing equations of the PCM model and the geometries selected to study the melting process under natural convection and thermocapillarity. The results of our simulations for natural convection and superposed thermocapillary driving are presented in Section 3, where we compare results for two Bond numbers and imposed temperatures. Finally, conclusions are provided in Section 4.

2 Governing equations and geometry

We have used two squared domain with sizes $h = 1$ and 2 cm. The left side of the squares is conductive held at a constant temperature T_h, greater than the melting temperature of the n-octadecane ($T_l = 26.1\,^\circ\mathrm{C}$), which is held initially at a solid phase ($T_i = 25\,^\circ\mathrm{C}$). The rest of the sides of the squared geometry are adiabatic. The top side is considered to be a free surface where the thermocapillary effects are acting. This configuration corresponds to a classical lateral heating.

2.1 Momentum equation

We consider the flow laminar, two-dimensional and incompressible. The governing equation expressing the balance of momentum has the vectorial form

$$\rho\left[\frac{\partial \mathbf{u}}{\partial t} + (\mathbf{u}\cdot\nabla)\,\mathbf{u}\right] = -\nabla p + \mu\nabla^2\mathbf{u} - \rho\, g\,[1-\alpha(T-T_{ref})]\,\mathbf{e_y} + \frac{C(1-f_l)^2}{\delta + f_l^3}\mathbf{u}, \quad (1)$$

where f_l is the local volume liquid fraction of the liquid phase of the PCM in a representative control volume. $\nabla = (\partial_x, \partial_y)$ and ∂_t are the spatial and temporal operators. T the temperature of a control volume that can contain pure solid ($f_l = 0$), liquid ($f_l = 1$) or a mixture of both phases ($0 < f_l < 1$); $\mathbf{u} = (u, v)$ is the fluid velocity; ρ is the density; μ is the dynamic viscosity, p is the pressure, g the magnitude of gravity acceleration, $\mathbf{e_y}$ an unit vector pointing in the vertical direction upwards, T_{ref} is a reference temperature where physical properties are given and α the thermal expansion coefficient. The bulk physical properties are supposed to be constant within the range of temperatures studied, with the exception of the density in the buoyancy term. We have neglected the viscous dissipation in the momentum equation since the dissipation number of natural convection satisfies $(g\alpha/c_l)h \ll 1$ [9] for the properties of n-octadecane (c.f. Tab. 1) and scale h used in this work.

Table 1. Thermophysical properties of n-octadecane. Values for the solid and liquid states are listed when distinguished in the equations of the PCM model of this work.

ρ ($\mathrm{Kg\,m^{-3}}$) [5]	776
μ ($\mathrm{N\,s\,m^{-2}}$) [5]	3.6×10^{-3}
$c_s \vert c_l$ ($\mathrm{J\,Kg^{-1}\,K^{-1}}$) [6]	1934|2196
$\lambda_s \vert \lambda_l$ ($\mathrm{W\,m^{-1}\,K^{-1}}$) [5]	0.358|0.13
γ ($\mathrm{Nm^{-1}\,K^{-1}}$) [7]	8.4×10^{-5}
$T_s \vert T_l$ (K) [5]	298.25|299.65
L ($\mathrm{J\,Kg^{-1}}$) [5]	243.5×10^3
α ($\mathrm{K^{-1}}$) [8]	9.1×10^{-4}

The last term in the momentum equation uses the Carman-Kozeny equation to model the solid/liquid interface as a porous mushy layer, whose porosity is given by the liquid fraction f_l. In this term $\delta \ll 1$ is a tiny constant to avoid division by zero without physical meaning, and C is a constant for the mushy region that depends on the PCM. We set the Darcy coefficient $C = 1.6 \times 10^6\,\mathrm{kg\,m^{-3}\,s}$, in compliance with previous works ([10]). When a control volume is completely liquid ($f_l = 1$) this term is null, like in a single phase fluid, when it is completely solid ($f_l = 0$) the term diverges and the velocity of the liquid becomes null, like in a solid. For intermediate values of f_l the PCM is within the mushy zone. This formulation allows to use the momentum equation in the whole domain without the complication of tracking the solid/liquid interface ([11]).

2.2 Energy equation

The thermal energy of the system comes from the contribution of the usual sensible heat, due to changes in temperature in the solid and liquid phases of the PCM, and from the latent heat content. Assuming the same density in each phase it can be expressed as a function of temperature as follows

$$\left[\frac{\partial}{\partial t} + \mathbf{u}\cdot\nabla\right] \rho\left((1-f_l)C_{pcm,s} + f_l\, C_{pcm,l}\right) T = \nabla\left((1-f_l)\lambda_{pcm,s} + f_l\,\lambda_{pcm,l}\right)\nabla T - \rho\, L\,\frac{\partial f_l}{\partial t} \tag{2}$$

where $C_{pcm,s}$ ($C_{pcm,l}$) and $\lambda_{pcm,s}$ ($\lambda_{pcm,l}$) are the specific heats and conductivities of the PCM in the solid (liquid) phase, averaged with the liquid fraction, and L is the latent heat of the solid/liquid phase change of the PCM.

The latent heat released by a control volume during the solid to liquid phase change depends on the melted PCM given by liquid fraction as $f_l\,\rho\,L$. As a consequence the coupling between the energy and momentum equation is given through the liquid fraction field f_l, which in turn depends on the temperature, the master variable of the phase change process. We model the liquid fraction in the mushy zone using a linear relationship between the solidus and liquidus temperatures

$$f_l = \begin{cases} 0, & T \le T_s \\ 1, & T \ge T_l \\ (T - T_s)/(T_l - T_s), & T_s < T < T_l. \end{cases} \tag{3}$$

2.3 Boundary conditions

The dependence of interfacial tension with the temperature at the free surface on top is approximated by the linear state equation

$$\sigma = \sigma_0 - \gamma(T - T_{ref}) \tag{4}$$

where σ_0 is the interfacial tension at the reference temperature T_{ref}, and $\gamma = -\partial\sigma/\partial T|_{T_{ref}}$ accounts for the dependence of interfacial tension with temperature.

The lateral heating along the free surface generates at Marangoni flow from the balance between shear force and surface tension

$$\mu\,\partial_z u = -\gamma \partial_x T \text{ at free surface.} \tag{5}$$

There is no penetration of the liquid on the free surface and the free surface is supposed to be adiabatic.

$$w = 0 \text{ at free surface} \tag{6}$$

$$\frac{\partial T}{\partial z} = 0 \text{ at free surface.} \tag{7}$$

We use the open source software OpenFOAM, based on finite volumes, to simulate the equations of the PCM model discussed above together the boundary conditions. We have validated the implementation of the Marangoni effect with results by Bergmann and Keller [12], who simulated the combined effect of buoyancy and thermocapillarity. We find a grid of 400×400 cells is enough to guarantee convergence of solutions.

3 Results

We have carried out simulations for both geometries with and without thermocapillary effects to evaluate their impact on the melting dynamics. We can estimate a Bond number $Bo = Ra/Ma = \alpha\rho\, g\, h^2/\gamma$, where Ra and Ma are the Rayleigh and Marangoni numbers respectively, assuming the domain filled with liquid PCM: ~ 8.3 for the small square and ~ 33 for the large one. Thus a major contribution of thermocapillarity is expected on the smaller domain.

Figure 1 shows the evolution of the volume fraction of melted PCM (global liquid fraction) for both geometries. In presence of natural convection, melting time at $T_h = 50\,^{\circ}\mathrm{C}$ for 1 cm square is 1378.1 s, and it is reduced to 1130 s (18%) when Marangoni driving is superposed. At higher temperature $T_h = 100\,^{\circ}\mathrm{C}$ melting time for natural convection is 426 s, and is reduced to 332 s (28.3%) when Marangoni driving is superposed. The melting time for $T_h = 100\,^{\circ}\mathrm{C}$ exhibits an improved relative difference of 10.3% compared to $T_h = 50\,^{\circ}\mathrm{C}$ when thermocapillarity is included. This shows that is not only the ratio between natural convection and thermocapillary convection, expressed by the Bond number, that dictates the melting rate: it is as well the average velocity of the liquid at the free surface that contributes to the magnitude of the advance of the solid/liquid interface. Thus, the speed of the melting front is affected by the rate of latent heat loss at the interface, the strength of convective motions driven by density gradients and driven by surface tension gradients.

The lower conductivity of the liquid phase with respect to the solid phase (c.f. Tab. 1) leads to a quick advance of the overall liquid fraction in the first stages of melting due to enhanced conductive transport within the solid phase of PCM. However, once the liquid phase of the PCM becomes more abundant the melting slows

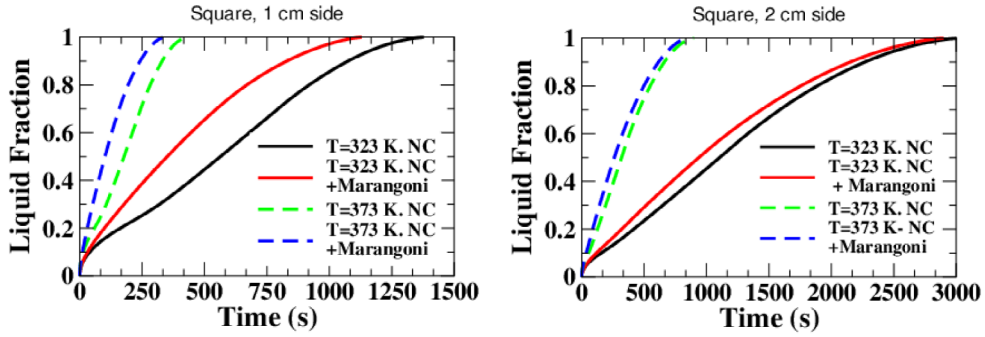

Fig. 1. Evolution of the global liquid fraction of n-octadecane for a square of size 1 cm (left) and 2 cm (right). Dashed lines correspond to $T_h = 323\,\mathrm{K}$, solid to $T_h = 373\,\mathrm{K}$. NC at the legends denotes Natural Convection.

down. Thus, for instance, it takes 59% of total melting time to liquefy the remaining 50% of solid PCM of 1 cm square at $T_h = 50\,^{\circ}\mathrm{C}$ when only natural convection acts. The melting of the first 50% is even faster when thermocapillary effects are included, taking 69% of the total melting time to liquefy the remaining 50% of PCM volume. This difference on heat transfer rate performance is enhanced by the fact that convective motions due to thermocapillarity appear quicker than convective motions due to natural convection, which requires about 1.6 mm of melted n-octadecane to destabilize the conductive state by buoyancy. Indeed for 2 cm square the relative strength of Marangoni effects is weaker, and the time difference between buoyancy and superposed to thermocapillarity cases to melt the first 50% is reduced to 4%. At $T_h = 100\,^{\circ}\mathrm{C}$ similar relative differences are found.

Figure 2 exhibits snapshots of streamlines and temperature fields across representative times of the melting process of n-octadecane for 1 cm square at $T_h = 50\,^{\circ}\mathrm{C}$ and $T_h = 100\,^{\circ}\mathrm{C}$. Times have been chosen to roughly exhibit 0.1, 0.5 and 0.8 of the global liquid fraction. For natural convection driving, the liquefied PCM flows from the hot left side and later cool down along the solid/liquid interface, returning and creating a single large convective cell. This global structure is conserved until complete melting of the PCM. Ascending hot melted PCM creates a faster advance of the interface near the hot adiabatic free surface, combined with a slow motion at the cooler bottom leads to an inclined interface which as time advances confines progressively the solid PCM on the right bottom corner. The detachment of the solid/liquid interface from the free surface is produced at both temperatures $\sim 58\%$ of the complete melting time. This melting dynamic is similar for $T_h = 50\,^{\circ}\mathrm{C}$ and $T_h = 100\,^{\circ}\mathrm{C}$.

As thermocapillary driving is superposed to natural convection (c.f. third and fourth rows of left block of Fig. 2) not only enhanced heat transfer rates result, as explained before, but also a qualitative change in the melting dynamics. First, there is a quick advance of the solid/liquid interface at the free surface that detaches from it at 130 s (12% of complete melting time) for $T_h = 50\,^{\circ}\mathrm{C}$, and 25 s (7.5% of complete melting time) for $T_h = 100\,^{\circ}\mathrm{C}$, liquefying the PCM at the upper half of the square. The reduction of time to detachment, from 12% to 7.5% is a consequence of the stronger thermocapillary flow with increasing T_h. Second, the convective patterns become more involved, with the creation of a thin convective cell below the free surface near of the left hot side at the early stages of melting, and the creation of two large counter-rotating cells at intermediate times. The smaller convective cell at the lower part carries cooler liquid from the top upwards along the solid/liquid interface.

Figure 3 exhibits snapshots for the temperature field and streamlines at representative times of 2 cm square, with $Bo = 33$. Convective motions are more involved with respect to 1 cm square due to greater buoyancy effects. Thus streamlines become less

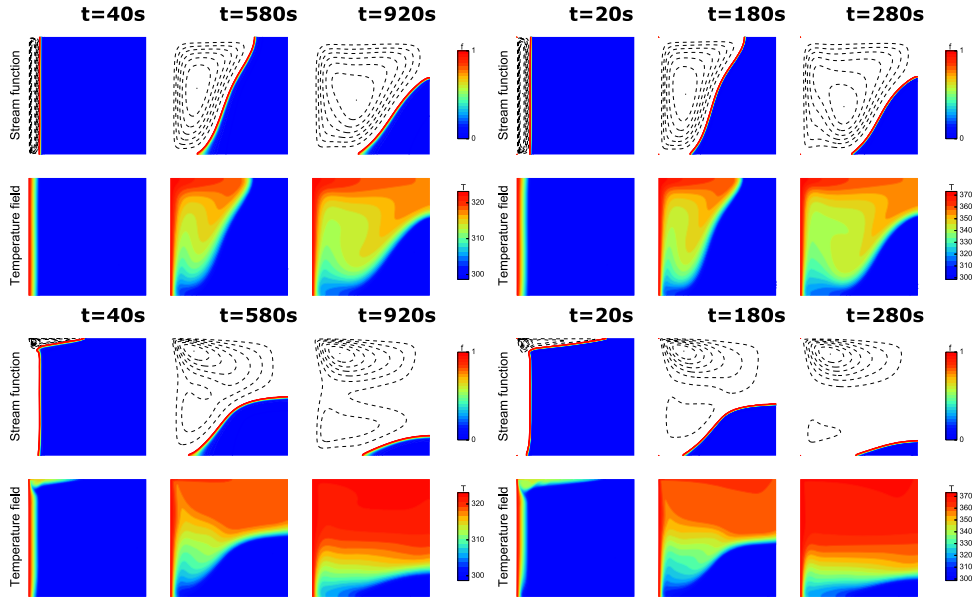

Fig. 2. Square of side 1 cm. Snapshots at representative times of the temperature field (second and fourth rows) and streamlines (first and third rows) for $T_h = 50\,^{\circ}\mathrm{C}$ (left block) and $T_h = 100\,^{\circ}\mathrm{C}$ (right block). Melting evolution is shown when only natural convection is acting (first and second rows), and when natural convection plus thermocapillarity are acting together (third and fourth columns).

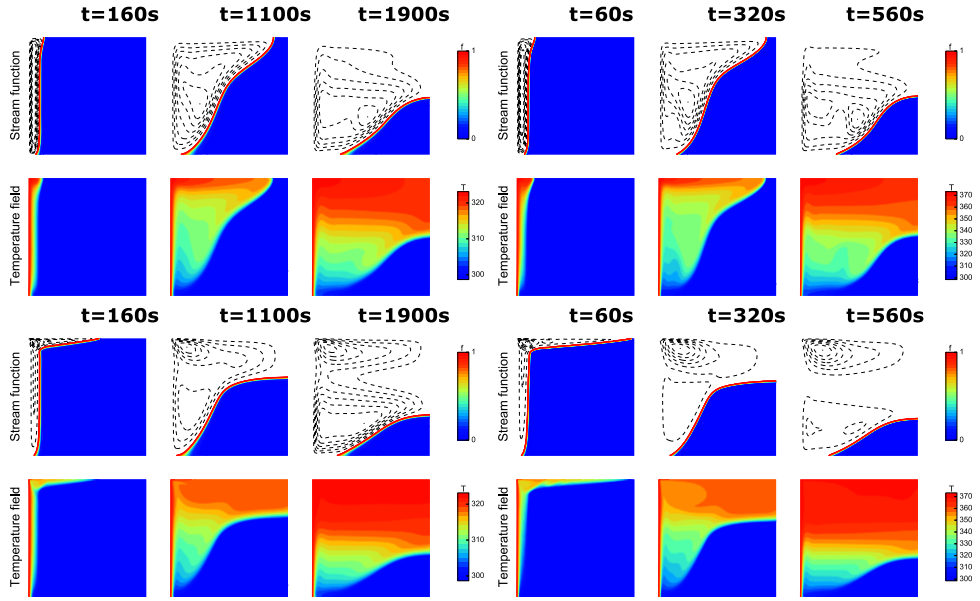

Fig. 3. Square of side 2 cm. Snapshots at representative times of the temperature field (second and fourth rows) and streamlines (first and third rows) for $T_h = 50\,^{\circ}\mathrm{C}$ (left block) and $T_h = 100\,^{\circ}\mathrm{C}$ (right block). Melting evolution is shown when only natural convection is acting (first and second rows), and when natural convection plus thermocapillarity are acting together (third and fourth columns).

smooth at all times, and at the latter stages of evolution new convective cells appear with respect to 1 cm square. However, overall dynamics of the solid/liquid front is similar as the discussed above for smaller Bond number. The weakening of the impact of thermocapillary flows at this large Bo on performance of heat transfer rate is appreciated comparing the effect of increasing T_h with respect to the previous case. Now the introduction of thermocapillary flows decreases the melting time to just 4.2% for $T_h = 50\,^{\circ}\mathrm{C}$, and 6.3% for $T_h = 100\,^{\circ}\mathrm{C}$, and the relative difference between both temperatures is 2.1%, compared with 10.3% for $Bo = 8.3$. In addition, the time to detachment of the solid/liquid interface from the free surface when thermocapillarity is included is 11% of the total melting time for $T_h = 50\,^{\circ}\mathrm{C}$, and 8% for $T_h = 100\,^{\circ}\mathrm{C}$. Thus the difference is reduced to 3%, compared to 4.5% for $Bo = 8.3$.

4 Conclusions

We have simulated the melting dynamics of the phase change material n-octadecane using an enthalpy-porosity formulation for the Navier-Stokes coupled to energy equations. Two squared geometries of 1 cm and 2 cm subjected to lateral heating, with respective Bond numbers 8.3 and 33 have been used to evaluate the influence of thermocapillary effects on heat transfer rate performance. We have calculated the global liquid fraction curves when convective motions are driven only by buoyancy and when thermocapillary flows are included. We find for $Bo = 8.3$ that adding thermocapillary effects decreases the total melting time 18% with $T_h = 50\,^{\circ}\mathrm{C}$ and 28% with $T_h = 100\,^{\circ}\mathrm{C}$. At $Bo = 33$ the influence of thermocapillary effects weakens with a decrease of the total melting time of 4.2% with $T_h = 50\,^{\circ}\mathrm{C}$ and 6.3% with $T_h = 100\,^{\circ}\mathrm{C}$.

Snapshots of stream functions and temperature fields have allowed following the evolution of melting dynamics. We find that overall evolution of solid/liquid interface is similar for both geometries and imposed external temperatures for buoyancy driving convection. The same happens when thermocapillary driving is superposed. However there are relevant qualitative and quantitative differences when buoyancy only, and added thermocapillarity are compared. The last case produces a very quick detachment of the solid/liquid front from the upper free surface.

From our results, we conclude that thermocapillary effects at small Bo are a very relevant mechanism to enhance the heat transfer rate on n-octadecane, especially when subjected to high external temperatures. Which happens, for instance, in applications of thermal control management on electronic devices. Importantly, this improvement of the heat transfer rate performance can be accomplished without adding complexity like embedding high conductivity metallic structures within the PCM, how is usually done.

Santiago Madruga acknowledges support by Erasmus Mundus EASED programme (Grant 2012-5538/004-001) coordinated by Centrale Supélec, and the Spanish Ministerio de Economía y Competitividad under Projects No. TRA2013-45808-R, No. ESP2013-45432-P and No. ESP2015-70458-P. Carolina Mendoza acknowledges support by the Ministerio de Economía y Competitividad under Project No. MTM2014-56392-R. We thank Gonzalo Sáez-Mischlich for code development and Pedro Mongelos for support with postprocessing.

References

1. S.A. Memon, Phase change materials integrated in building walls: A state of the art review, Renew. Sustain. Energy Rev. **31**, 870 (2014)
2. X. Gui, D. Tang, S. Liang, B. Lin, X. Yuan, Influence of void ratio on thermal performance of heat pipe receiver, Int. J. Heat Fluid Flow **33**, 109 (2012)

3. T.Y. Kim, B.S. Hyun, J.J. Lee, J. Rhee, Numerical study of the spacecraft thermal control hardware combining solid-liquid phase change material and a heat pipe, Aerosp. Sci. Technol. **27**, 10 (2013)
4. D. Fernandes, F. Pitié, G. Cáceres, J. Baeyens, Thermal energy storage: How previous findings determine current research priorities, Energy **39**, 246 (2012)
5. C.J. Ho, J.Y. Gao, Preparation and thermophysical properties of nanoparticle-in-paraffin emulsion as phase change material, Int. Commun. Heat Mass Transf. **36**, 467 (2009)
6. E.M. Alawadhi, Thermal analysis of a building brick containing phase change material, Energy Build. **40**, 351 (2008)
7. D.R. Lide, ed., *CRC Handbook of Chemistry and Physics*, 84th edn. (CRC Press, 2003)
8. N.S. Dhaidan, J.M. Khodadadi, T. Al-Hattab, S.M. Al-Mashat, Experimental and numerical investigation of melting of phase change material/nanoparticle suspensions in a square container subjected to a constant heat flux, Int. J. Heat Mass Transf. **66**, 672 (2013)
9. B. Gebhart Effects of viscous dissipation in natural convection, J. Fluid Mech. **14**, 225 (1962)
10. S.S. Sebti, M. Mastiani, H. Mirzaei, A. Dadvand, S. Kashani, S.A. Hosseini, Numerical study of the melting of nano-enhanced phase change material in a square cavity, J. Zhejiang Univ. Sci. A **14**, 307 (2013)
11. C. Beckermann, R. Viskanta, Natural convection solid/liquid phase change in porous media, Int. J. Heat Mass Transf. **31**, 35 (1988)
12. T.L. Bergman, J.R. Keller. Combined buoyancy, surface tension flow in liquid metals. Numerical Heat Transfer **13**, 49 (1988)